

# SHALLOW STRUCTURE IN THE KAROO BASIN, SOUTH AFRICA, INFERRED FROM A NEAR VERTICAL REFLECTION SEISMIC PROFILE

J. STANKIEWICZ

Deutsches GeoForschungsZentrum GFZ, Telegrafenberg, Potsdam, 14473, Germany

e-mail: jacek@gfz-potsdam.de

© 2011 December Geological Society of South Africa

## ABSTRACT

A Near Vertical Reflection seismic profile from Beaufort West to Klaarstroom was carried out using controlled source vibroseis sweeps and a rolling spread of recording geophones. Arrivals of refracted P- and S-waves generated in the sweeps were manually picked. 2-D travel time tomography was used to compute P-wave and S-wave velocity variations for depths down to ~300 m beneath the profile. Checkerboard tests illustrate the resolution of the velocity models. A probabilistic classification approach was used in an attempt to identify lithological classes based on observed P- and S-wave velocities. Two classes were identified, but they do not correspond to different geological formations. Thus the variations of seismic velocities due to pressure and compaction are greater inside a given formation than between different formations. The subsurface down to a depth of 50 to 100 metres shows very little variation in S-wave velocity,  $2.2 \pm 0.1$  km/s, irrespective of the underlying geological formation. Directly below this zone variations in P- and S-wave velocities are observed, where the  $V_p/V_s$  ratio is approximately 2. Care must thus be taken when attempting to classify lithologies using statistical distribution of geophysical parameters – systematic variations inside a single geological unit can be more significant than between separate geological formations.

## Introduction

A ~100 km Near Vertical Reflection (NVR) seismic profile from Beaufort West to Klaarstroom (Figure 1) was carried out by the Council of Geoscience in 1992. However, the results of the experiment have not been presented until Loots et al. (2010). The data collected in this experiment were incorporated into the Inkaba yeAfrica project (de Wit and Horsfield, 2006), to complement numerous seismic experiments carried out along the Agulhas-Karoo Geoscience Transect in the framework of the project (e.g. Bräuer et al., 2007; Stankiewicz et al., 2008; Parsiegla et al., 2009). Along the profile 683 vibroseis sweeps were used as sources, spaced every ~150 m. For each source 180 receiver stations, each made up of 24 SM-4B 10 Hz geophones, were used. The receivers were spaced every ~50 m, with ~90 on either side of the active source, giving a maximum offset of ~4.5 km. A total of 2011 receiver locations were used during the experiment. The sampling rate used was 4 ms. While the primary aim of the experiment was to observe seismic reflections from crustal structures (Loots et al., 2010), arrivals of refracted P- and S-waves were also observed. This study performs an analysis of the travel times of these phases, and uses travel time tomography to map the local variations in the seismic velocities, as well as Poisson's ratio, down to a depth of ~300 m along the profile. These velocity models are used in an attempt to identify different lithological classes, and we demonstrate how care must be taken when such classifications are performed.

## Profile Setting

The geological setting of the seismic line is shown in Figure 1. The southern end of the line coincides with the

tectonic front of the Cape Fold Belt (CFB). This east-west striking mountain chain has been extensively deformed between 280 and 230 Ma (de Wit, 1992; Hälbig, 1992), and today consists of structurally complex northward verging overturned folds. North from here, the sedimentary rocks of the Karoo Basin are more gently folded. The Karoo Basin is a retroarc foreland basin adjacent to the CFB (Cole, 1992). The oldest rocks in the so-called Karoo Supergroup are the Upper Paleozoic glacial tillites of the Dwyka Group and the siliciclastic turbidite deposits of the Ecca Group – these are both encountered along the southern 30 km of our seismic profile. Farther north the profile crosses the siliciclastic sandstones and mudstones of the Beaufort Group – here the amount folding is very small, and the formations are nearly horizontal at the Great Escarpment, the front of which marks the northern end of the seismic line.

An important geophysical feature intersecting the profile is the Beattie Magnetic Anomaly (BMA). First detected by Beattie (1909), this positive static magnetic anomaly stretches more than 1000 km in roughly east-west orientation. The source of the anomaly remains unclear (e.g., de Beer and Gough, 1980; Pitts et al., 1992; Harvey et al., 2001; Weckmann et al., 2007), but the shallowest estimates put the source at a depth of 7 km – much deeper than can be resolved here.

## Data Processing and Tomography

P-wave arrivals could be clearly seen in the majority on the recorded traces, and 74,639 arrival times were manually picked. S-waves arrivals were not always present, and their quality was usually inferior to that of P-wave arrivals. This is likely due to interactions with P-coda, the ground roll and converted phases.

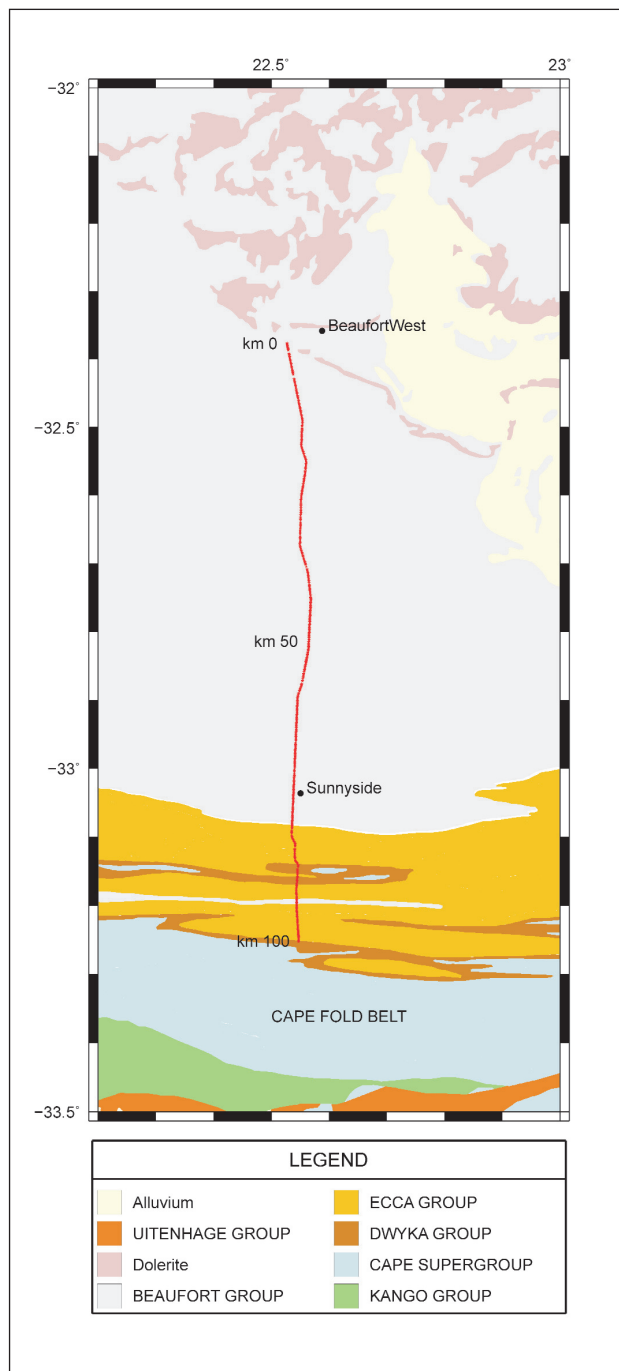


**Figure 1.** The seismic profile analysed here (shot locations as red dots) on a simplified geological map from Volquardsen et al (1984). Locations of km 0, 50, and 100 correspond to cross-sections in Figures 3, 4 and 6.

Nonetheless, we could confidently identify 9,703 S-wave arrival times. Figure 2 shows an example of data recorded from a single shot, with both P- and S-wave signals clearly visible.

A 2-dimensional tomographic inversions algorithm was used to identify variations in P- and S-wave velocities beneath the profile. To achieve this, the source and receiver locations must be projected onto a straight line, and the space under the profile divided into

rectangular cells. An initial velocity model needs to be provided by assigning a particular velocity at each cell. Synthetic travel times between available source-receiver pairs are then calculated, and compared to the real (picked) travel times. The velocity values assigned to the cells are then iteratively adjusted using the finite difference approach (Vidale, 1988) to minimise the misfit. This method was further modified by Zelt and Barton (1998) to make high velocity contrasts easier to detect. These authors released a software package FAST (First Arrival Seismic Tomography), which was used in our study.

While performing tomographic inversion, it is important to be aware of the non-uniqueness of the solution, especially its possible dependence on the starting model. To minimise the impact of the starting model, the approach developed by Ryberg et al (2007) is used here. This method uses FAST on a very coarse cell grid, and then resamples the result of the inversion onto a slightly finer grid. This is then used as a starting model for the inversion performed on the new grid. After five iterations, a fine-grid velocity model is obtained. In this study we considered cell size of 400 m length against 2 m height to be appropriate for the final inversion – such a high aspect ratio is necessary because of the shallow ray penetration depth compared to the profile length.

## Results

The P- and S- velocity models are shown in Figure 3. The P-wave model has a velocity range between 3.5 and 5.5 km/s, and the S-wave model between 1.8 and 3.0 km/s. The rms misfit between picked and synthetic travel times are 4.18 and 7.00 ms for the P- and S-wave models, respectively. The rms for the P-wave model approaches the sampling rate of 4 ms, which marks a theoretical minimum for the misfit, implying excellent resolution. For the S-wave model the misfit is higher due to much fewer travel times being available.

A number of inversions were performed using different starting models, and the results were found to be independent of these. The models also did not change significantly when inversion parameters were varied, as long as these were kept reasonable. The models in Figure 3 are thus presented with confidence that they reflect the real velocity variations along and beneath the profile. For the presented models smooth regularization was used ( $\alpha = 0.99$  in FAST), while the relative importance of vertical to horizontal smoothness (parameter  $sz$  in FAST) was set at 0.25.

To further evaluate the resolution of the presented velocity models checkerboard tests were performed. In these tests artificial velocity models consisting of alternating positive and negative velocity anomalies are constructed. Synthetic travel times between the available station-receiver pairs are then calculated using forward modeling. It is important to only use station-receiver pairs which yielded an observed travel time used in inversion. These travel times are then inverted from a

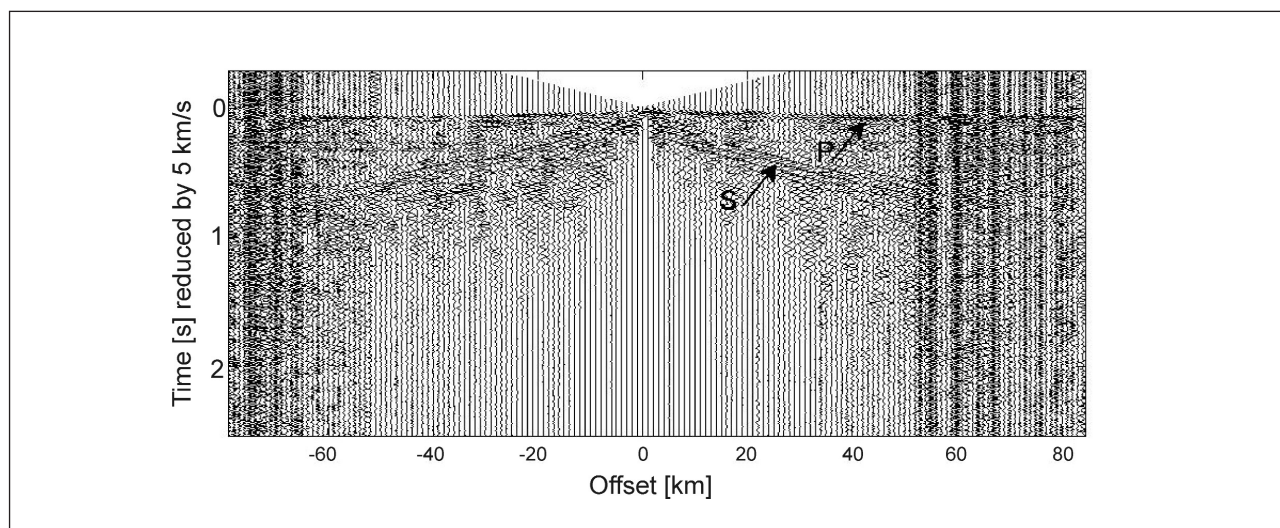


**Figure 2.** Example of the seismic traced recorded by a single shot. The y-axis (time) is time reduced by 5 km/s. Thus P-wave arrivals appear near-horizontal. S-waves arrivals are also visible, though less clearly.

1-D (velocity uniformly increasing with depth) starting model. Where checkerboard anomalies can be recovered, the implication is that at that location an anomaly with a size and amplitude corresponding to those of the input anomalies can be resolved. Care must be taken with interpreting these results – a review of this method by Lévêque et al. (1993) shows how misinterpretations can occur.

Examples of these recovery tests for the models presented here are shown in Figure 4. The P-wave model is very well resolved. The S-wave model needs to be interpreted with more caution – this is to be expected from the significantly smaller number of rays available. Nonetheless, the main features of the model can be treated with confidence.

### Interpretation

An efficient way of interpreting a seismic profile cross-section is a joint interpretation of velocity models of different types of seismic waves. By including both P- and S-wave velocity models in the analysis, more information can be extracted from the models than by treating them individually. Such an interpretation can be treated as a classification problem (e.g. Schalkoff, 1992). This approach involves categorising objects by assigning them to classes defined by limits of the measured physical parameters, in our case the various seismic velocities. This technique has been successfully used to interpret P- and S-wave velocity models computed in other NVR seismic profiles (e.g. Bauer et al, 2003).

When two independent parameters, are available, as is the case in this study, classification can be performed manually. To perform this, a probability density function (pdf) of the parameter distribution must be calculated. For every given data point at which both P- and S-velocities are defined the pdf for that point is a bivariate Gaussian function centred at the given velocity

values, and with a width corresponding to the uncertainties associated with these velocities. The uncertainties were estimated by using the relative density of ray coverage. The pdf for the complete models is the sum of individual pdfs. A high value for this function indicates a high probability of a point in models space having the corresponding values for P- and S-wave velocities. The mathematical details involved can be found in Bauer et al. (2003).

Following the computation of the pdf, a manual cluster analysis is performed to identify various classes. This involves identifying topologically continuous regions, or clusters, of high probability. Since the pdf is defined as a sum of bivariate Gaussian functions, coherent clusters should also closely resemble Gaussian functions. For this reason they are often represented by ellipses centred at the highest probability in the cluster, with the axes of the ellipse corresponding to the width of the Gaussian function representing the cluster (Muñoz et al., 2010). These ellipses are picked manually. Neural network techniques have been developed to identify clusters automatically (Bauer et al., 2008), and are necessary to perform classification when more than two input parameters are available, as functions of three or more parameters are difficult to image. However, with two input parameters, as is the case in our study, final results of manual cluster identification and of the neural network approach are very similar (Stankiewicz et al., 2010).

The final step in such analysis is remapping the clusters into model space. This is done by taking the parameter (P- and S-velocity) values at each model grid cell, and assigning the cell to the cluster with matching, or closest, values. This provides the spatial distribution of the identified classes.

The pdf correlating the P- and S-wave velocities presented in this study is shown in Figure 5.

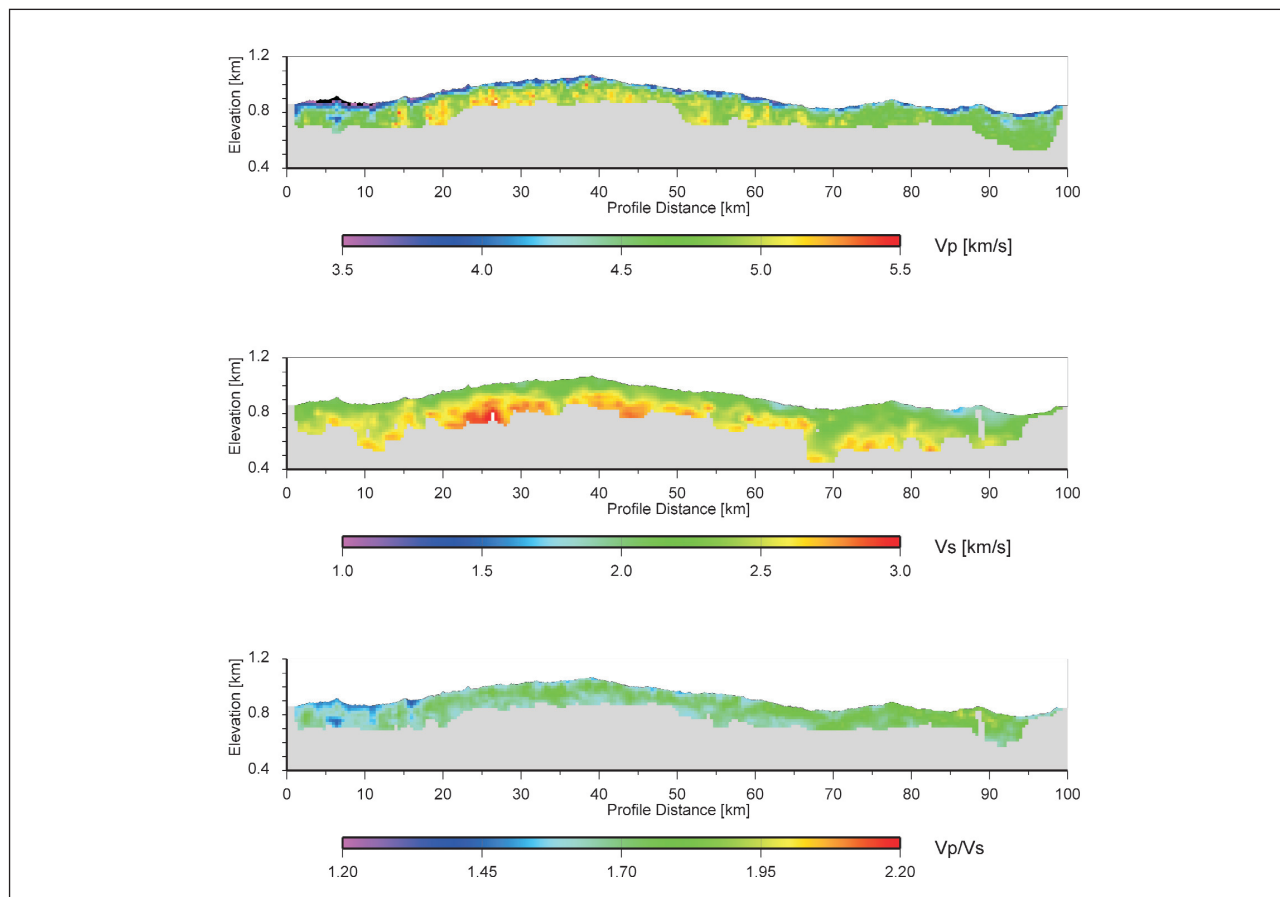


**Figure 3.** Velocity models computed for P-waves (top) and S-waves (middle), as well the  $V_p/V_s$  ratio (bottom). Profile km 0 corresponds to the northern end of the profile.

Two ellipses have been drawn to highlight the two obvious clusters of enhanced probability. The more prominent cluster covers almost the entire range of observed S-wave velocities ( $\sim 2.1$  to  $2.7$  km/s), and associates P-wave velocities in the range  $\sim 4.4$  to  $5.3$  km/s with them, with the expected trend of P velocities increasing with S. The ratio of P-wave to S-wave velocities is very close to 2 – this corresponds to Poisson's ratio of  $1/3$ . The second cluster covers a very narrow range of S-wave velocities ( $\sim 2.1$  to  $2.3$  km/s), but a wide range for those of P-waves ( $3.6$  to  $4.4$  km/s). Poisson's ratio is thus related to the P-wave velocity, varying from  $0.24$  to  $0.35$ .

The clusters are remapped into model space in Figure 6, with the prominent cluster (characterised by higher P-wave velocities) in red and the secondary one in blue. As the remapped regions are topologically continuous, we can conclude we have identified two real regions defined by ranges of seismic velocities. The secondary cluster, defined by S-wave velocities around  $2.2$  km/s and P-wave velocities slower than  $4.4$  km/s, corresponds to the uppermost 50 to 100 metres beneath the profile. It is underlain by the class defined by faster velocities, where P- and S-wave velocities are approximately proportional to each other. It is clear that the two classes do not correspond to

different geological formations – Figure 6 does not correlate with Figure 1, or any reasonable geological cross-section, which might be inferred from it. The classes thus represent petrophysical layers, not defined by composition, but other effects such as compaction or fluid saturation. As P-velocity significantly increases when measured below the water table, while S-velocity remains unaffected (e.g., Nur and Simmons, 1969), fluid saturation cannot explain the velocities observed here. Compaction and pressure thus appear to be the factors determining the velocities, with the S-wave velocities only dependent on them at depths exceeding 50 metres.

While two classes we identified along the profile, it is necessary to observe velocity variations inside each class. Some P-wave variations are present in the shallow class – the southernmost 30 km (profile km 70 to 100 in Figure 3) are characterised by slower velocities, not exceeding  $4.5$  km/s. This segment corresponds to the outcrop of the Ecca Group, where slow P-wave velocities have been observed in other profiles (Bräuer et al., 2007). The outcrop of the Dwyka Group is likely to be too narrow to have a seismic signature.

Another feature clearly visible in Figure 3 is the zone of higher velocities for both P- and S-waves between profile km 15 and 55. This cannot be explained by surface geology alone, as the northernmost 70 km of

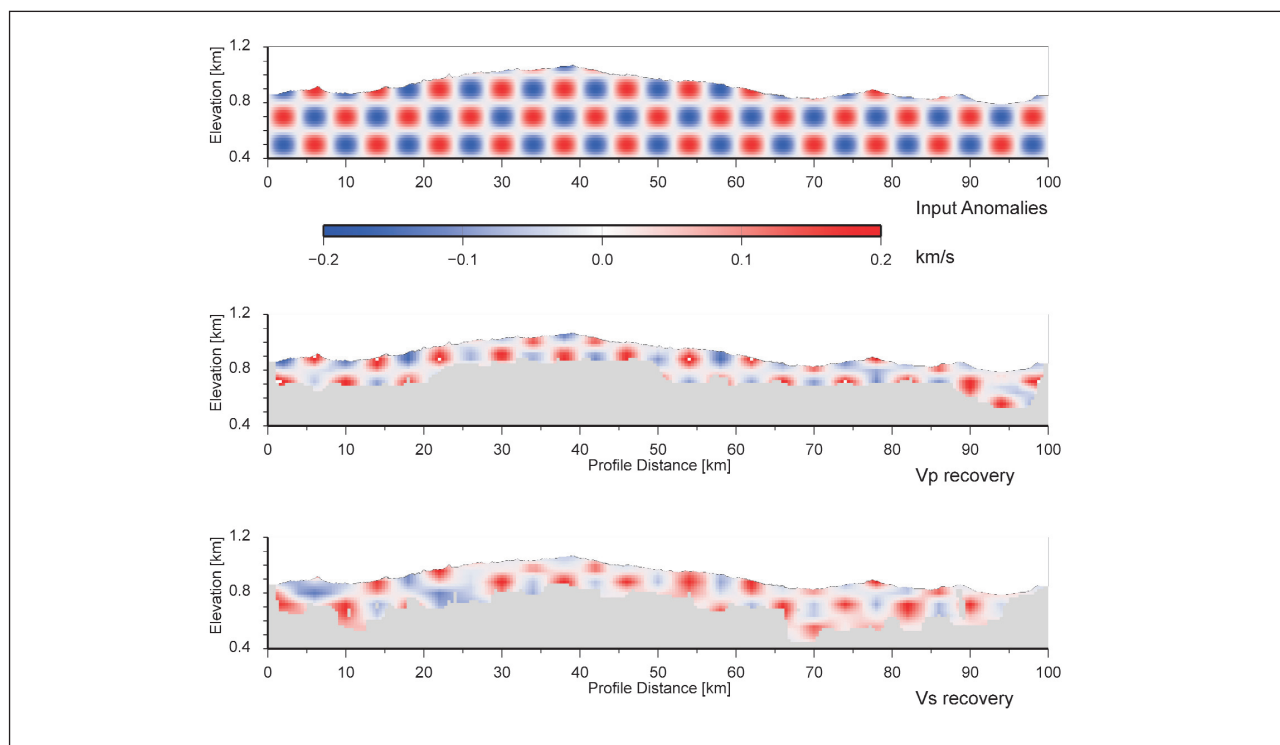


**Figure 4.** Example of checkerboard tests performed to gauge the resolution of the models in Figure 3. Top panel shows the input anomalies (400 m long, 200 m high, maximum perturbation 0.2 km/s), the middle panel the recovery using available P-wave travel times, and bottom panel for the S-waves. See text for more discussion

the profile cross only the Beaufort Group. However, the high velocities underlie topographically higher ground. Thus our results are consistent with the explanation that denser rocks underlie this section of the profile – these would require more time to erode, resulting in the observed topographic high.

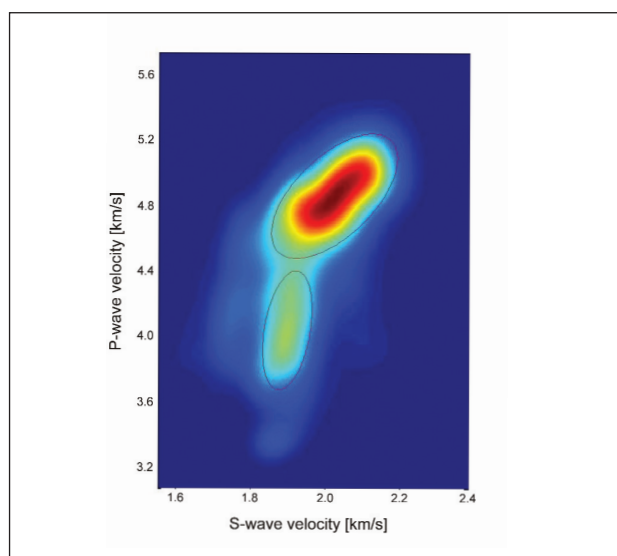


**Figure 5.** The probability density function of pairs of P- and S-wave velocity values co-existing. Warm colours correspond to enhanced probabilities. The two prominent clusters have been highlighted by ellipses.

## Conclusions

Travel time tomography was used to compute P- and S-wave velocity variations along a 100 km long controlled source seismic profile from Beaufort West to Klaarstroom. The maximum source-receiver offset used during the experiment made it possible to measure velocities to depths not exceeding 300 metres. To jointly interpret the two independent velocity models, the probabilistic classification approach was used in an attempt to resolve separate lithological classes. Two classes were identified, but they do not correspond to different geological formations. This is likely to be due to variations of seismic velocities inside a given formation being greater than between different formations. The conclusions of this study can be summarised as follows:

- The subsurface beneath the entire profile down to a depth of 50 to 100 metres shows very little lateral variation in S-wave velocity,  $2.2 \pm 0.1$  km/s, irrespective of the underlying geological formation.
- In this shallow zone slower P-wave velocities distinguish the Ecca Group exposure from the faster velocities observed in the Beaufort Group.
- Directly below this zone of near-constant S-wave velocity variations in P- and S-wave velocities are observed, with a good correlation between them – the  $V_p/V_s$  ratio is approximately 2.
- Care must be taken when attempting to classify lithologies using statistical distribution of geophysical parameters – systematic variations inside a single

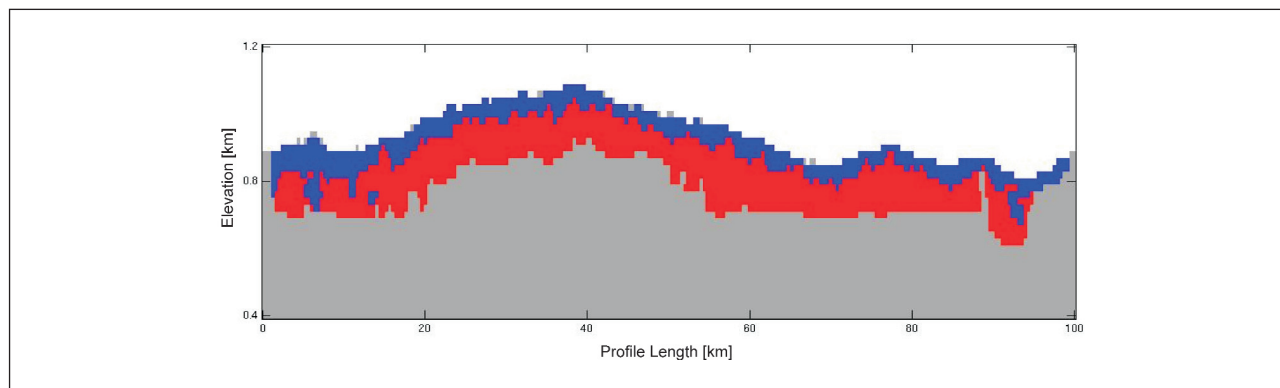


**Figure 6.** Remapping the clusters from Figure 5 into model space. The dominant, high velocity ( $V_p$ : 4.4 to 5.3 km/s,  $V_s$ : 2.1 to 2.7 km/s) cluster in red, the secondary cluster ( $V_p$ : 3.6 to 4.4 km/s,  $V_s$ : 2.1 to 2.3 km/s) in blue.

geological unit can be more significant than between separate geological formations.

### Acknowledgments

The seismic profile is interpreted in the framework of the collaboration between the Council for Geoscience and Deutsches GeoForschungsZentrum Potsdam. In particular the involvement of Klaus Bauer, Benjamin Bräuer, Ray Durrheim, Leticia Loots, Trond Ryberg, Ariane Siebert, Robert Trumbull and Michael Weber is acknowledged. Tomography study is funded by the Helmholtz-Russia Joint Research Groups (HRJRG-110). This is Inkaba yeAfrica contribution 42.

### References

- Bauer, K., Schulze, A., Ryberg, T., Sobolev, S.V. and Weber, M. H., 2003. Classification of lithology from seismic tomography: A case study from the Messum igneous complex, Namibia. *Journal of Geophysical Research*, 108, B3, 2152.
- Bauer, K., Pratt, R.G., Haberland, C. and Weber, M., 2008. Neural network analysis of crosshole tomographic images: The seismic signature of gas hydrate bearing sediments in the Mackenzie Delta (NW Canada). *Geophysical Research Letters*, 35, L19306.
- Beattie, J.C., 1909. Report of a magnetic survey of South Africa. Royal Society of London Publication, Cambridge University Press, London, U.K., 235pp.
- Bräuer, B., Ryberg, T. and Lindeque, A., 2007. Shallow seismic velocity structure of the Karoo Basin, South Africa. *South African Journal of Geology*, 110, 439–448.
- Cole, D.I., 1992. Evolution and development of the Karoo Basin. In: M.J. De Wit and I.G.D. Ransome (Editors), *Inversion Tectonics of the Cape Fold Belt, Karoo and Cretaceous Basins of Southern Africa*, Balkema, Rotterdam, The Netherlands, 87–99.
- de Beer, J.H. and Gough, D.I., 1980. Conductive structures in southernmost Africa: a magnetometer array study. *Geophysical Journal of the Royal Astronomical Society*, 63, 479–495.
- de Wit, M.J., 1992. The Cape Fold Belt: A challenge for an integrated approach to inversion tectonics. In: M.J. De Wit and I.G.D. Ransome (Editors), *Inversion Tectonics of the Cape Fold Belt, Karoo and Cretaceous Basins of Southern Africa*, Balkema, Rotterdam, The Netherlands, 3–12.
- de Wit, M.J. and Horsfield, B., 2006. Inkaba yeAfrica Project surveys sector of Earth from core to space. *EOS*, 87, 11.
- Hälbich, I.W., 1992. The Cape Fold Belt Orogeny: State of the art 1970s–1980s. In: M.J. De Wit and I.G.D. Ransome (Editors), *Inversion Tectonics of the Cape Fold Belt, Karoo and Cretaceous Basins of Southern Africa*, Balkema, Rotterdam, The Netherlands, 141–158.
- Harvey, J.D., de Wit, M.J., Stankiewicz, J. and Doucoure, C.M., 2001. Structural variations of the crust in the Southwestern Cape, deduced from seismic receiver functions. *South African Journal of Geology*, 104, 231–242.
- Lévêque, J.-J., Rivera, L. and Wittlinger, G., 1993. On the use of checkerboard test to assess the resolution of tomographic inversions. *Geophysical Journal International*, 115, 313–318.
- Loots, L., Durrheim, R.J. and Ryberg, T., 2010. Investigation of the crust in the Southern Karoo using the seismic reflection technique. *Inkaba ye Africa 7th Annual Workshop Abstract*, 42pp.
- Muñoz, G., Bauer, K., Moeck, I., Schulze, A. and Ritter, O., 2010. Exploring the Gross Schoenebeck (Germany) geothermal site using statistical joint interpretation of magnetotelluric and seismic tomography models. *Geothermics*, 39, 35–45.
- Nur, A. and Simmons, G., 1969. The effect of saturation on velocity in low porosity rocks. *Earth and Planetary Science Letters*, 8, 183–193.
- Parsieglä, N., Stankiewicz, J., Gohl, K., Ryberg, T. and Uenzelmann-Neben, G., 2009. Southern African continental margin: Dynamic processes of a transform margin. *Geochemistry, Geophysics, Geosystems*, 10(3), Q03007.
- Pitts, B.E., Maher, M.J., de Beer, J.H. and Gough, D.I., 1992. Interpretations of magnetic, gravity and magnetotelluric data across the Cape Fold Belt and Karoo Basin. In: M.J. De Wit and I.G.D. Ransome (Editors), *Inversion Tectonics of the Cape Fold Belt, Karoo and Cretaceous Basins of Southern Africa*, Balkema, Rotterdam, The Netherlands, 27–32.
- Ryberg, T., Weber, M.H., Garfunkel, Z. and Bartov, Y., 2007. The shallow velocity structure across the Dead Sea Transform fault, Arava Valley, from seismic data. *Journal of Geophysical Research*, 112, B08307.
- Schalkoff, R., 1992. *Pattern Recognition: Statistical, Structural, and Neural Approaches*, John Wiley and Sons, New York, 364pp.
- Stankiewicz, J., Parsieglä, N., Ryberg, T., Gohl, K., Weckmann, U., Trumbull, R. and Weber, M., 2008. Crustal structure of the southern margin of the African continent: Results from geophysical experiments. *Journal of Geophysical Research*, 113, B10313.
- Stankiewicz, J., Bauer, K. and Ryberg, T., 2010. Lithology classification from seismic tomography: additional constraints from surface waves. *Journal of African Earth Science*, 58, 547–552.
- Vidale, J.E., 1988. Finite-difference calculation of travel times. *Bulletin of the Seismological Society of America*, 78, 2062–2076.
- Volquardsen, U., Wilkinson, K.J., Coetzee, L.E. and Steyn, J.H., 1984. *Geological Map of South-West Africa, 1:1 000 000*. Council of Geoscience, Pretoria, South Africa.
- Weckmann, U., Ritter, O., Jung, A., Branch, T. and de Wit, M.J., 2007. Magnetotelluric measurements across the Beattie magnetic anomaly and the Southern Cape Conductive Belt, South Africa. *Journal of Geophysical Research*, 112, B05416.
- Zelt, C.A. and Barton, P.J., 1998. Three-dimensional seismic refraction tomography: A comparison of two methods applied to data from the Faeroe Basin. *Journal of Geophysical Research*, 103(B4), 7187–7210.

Editorial handling: R.B. Trumbull